Resistivity scaling due to electron surface scattering in thin metal layers

Tianji Zhou and Daniel Gall
Department of Materials Science, Rensselaer Polytechnic Institute, Troy, New York 12180, USA

(Received 11 December 2017; revised manuscript received 14 February 2018; published 5 April 2018)

The effect of electron surface scattering on the thickness-dependent electrical resistivity ρ of thin metal layers is investigated using nonequilibrium Green's function density functional transport simulations. Cu(001) thin films with thickness $d = 1 - 2$ nm are used as a model system, employing a random one-monolayer-high surface roughness and frozen phonons to cause surface and bulk scattering, respectively. The zero-temperature resistivity increases from $9.7 \pm 1.0\,\mu\Omega\,\text{cm}$ at $d = 1.99$ nm to $18.7 \pm 2.6\,\mu\Omega\,\text{cm}$ at $d = 0.90$ nm, contradicting the asymptotic $T = 0$ prediction from the classical Fuchs-Sondheimer model. At $T = 900$ K, $\rho = 5.8 \pm 0.1\,\mu\Omega\,\text{cm}$ for bulk Cu and $\rho = 13.4 \pm 1.1$ and $22.5 \pm 2.4\,\mu\Omega\,\text{cm}$ for layers with $d = 1.99$ and 0.90 nm, respectively, indicating an approximately additive phonon contribution which, however, is smaller than for bulk Cu or atomically smooth layers. The overall data indicate that the resistivity contribution from surface scattering is temperature-independent and proportional to $1/d$, suggesting that it can be described using a surface-scattering mean-free path λ_s for 2D transport which is channel-independent and proportional to d. Data fitting indicates $\lambda_s = 4 \times d$ for the particular simulated Cu(001) surfaces with a one-monolayer-high surface roughness. The $1/d$ dependence deviates considerably from previous $1/d^2$ predictions from quantum models, indicating that the small-roughness approximation in these models is not applicable to very thin (<2 nm) layers, where the surface roughness is a considerable fraction of d.

DOI: 10.1103/PhysRevB.97.165406

I. INTRODUCTION

Electron transport in thin metallic films including the prediction of the resistivity ρ as a function of layer thickness d continues to be of great scientific interest [1–13]. Electron scattering at film surfaces [14–19] is particularly important as it causes an increase in ρ with decreasing thickness [20–26] that has also garnered technological interest as it impedes integrated circuit downscaling [27,28]. This resistivity size effect due to surface scattering is described by the classical Fuchs-Sondheimer (F-S) model [1,2], which employs Boltzmann transport and assumes that electron relaxation only occurs in the bulk, while partially diffuse scattering at the surfaces is accounted for by boundary conditions. The bulk scattering is quantified by the bulk mean-free path λ which is typically dominated by phonon scattering and is therefore temperature-dependent, while surface scattering is described by a phenomenological specularity parameter p that defines the probability for specular vs diffuse electron reflection at the surfaces. The F-S model describes experimental data well for layer thicknesses that are comparable to or larger than λ, but consistently underestimates the measured resistivity for layers with $d < 20$ nm [16,18,20,22,23,29–35]. Moreover, in the limit of high-purity films at low temperature, i.e., $\lambda \rightarrow \infty$, the F-S model predicts a vanishing thin-film resistivity since surface scattering alone cannot relax carriers within the F-S model. This intrinsic limitation of the F-S model [3] originates from two approximations that are not necessarily satisfied at small thickness, in particular (i) the electronic structure is bulklike, and (ii) the surface scattering occurs exactly at the surface. Later studies have proposed other models to replace the F-S model [3,4,5,7,12]. They apply a two-dimensional transport description with quantized vertical wave vector components, leading to an electronic structure with subbands and an in-plane conductivity defined by the sum over all conduction channels [5]. Within that framework, surface scattering can be described by a mean-free path λ_s that quantifies electron relaxation due to surface scattering [5], contrary to the specularity parameter within the FS model which describes a boundary effect without electron relaxation. The resistivity in the limit of small thickness and/or low temperature from these quantum mechanical models [3,4,5,7] is proportional to $1/d^2$. This is in direct contradiction to the F-S model which predicts $\rho \propto 1/[d\ln(\lambda/d)]$ for small d and/or large λ. The disagreement at small d suggests the breakdown of the F-S model and motivates resistivity studies that determine the ρ vs d dependence at small thicknesses. Such studies also provide quantitative insight and corresponding benchmark data for metal nanowire applications including the continued downscaling of integrated circuits.

First-principles simulations that explicitly account for the atomic level structure and associated electronic structure of the thin film are expected to yield correct transport data for very thin films and nanowires [15,21,36–42]. They do not directly provide a functional form for ρ as a function of, for example, layer thickness, surface roughness, bulk (phonon) scattering, or metal element. Nevertheless, we use in this study this approach to numerically determine the ρ vs d relationship for thin Cu(001) layers using a large number of individual transport simulations. A key strength of this method is full control over the parameters that determine electron scattering. For example, a specific surface roughness [15,36,43] or atomic displacements (to simulate temperature) [44,45] can be easily constructed and kept constant while varying geometrical pa-

rameters of the conductor, providing a direct path to determine the resistivity from the calculated ballistic conductance and ultimately the resistivity as a function of any desired structural parameter. Correspondingly, in a second step, the simulated data can be directly compared to model predictions to evaluate existing or newly developed functional forms for the resistivity size effect.

In this paper, we present results from first-principles calculations of electron transport in 1–2 nm thick Cu(001) films, employing nonequilibrium Green's function (NEGF) density functional theory (DFT) calculations. The chosen thickness range is large enough so that the charge distribution in the film center is bulklike, but is still comparable to the Fermi wavelength in Cu (∼0.46 nm), such that quantum effects cannot be neglected. Electron surface scattering is facilitated by a 50%-coverage surface monolayer that represents a random atomic-level roughness. The zero-temperature resistivity is purely caused by this surface scattering, while finite-temperature bulk scattering is included with a frozen-phonon approach. Resistivities at both temperatures are calculated as a function of film thickness, providing ρ vs d data that can be directly compared to predictions of the existing models. The overall results indicate that the resistivity contribution due to surface scattering is proportional to $1/d$, in direct contradiction to the classical F-S model. In addition, the data also deviate strongly from the $1/d^2$ prediction from more recent quantum models, suggesting that the small-roughness approximation is not applicable and that the surface roughness also affects electron scattering within the layer.

II. COMPUTATIONAL PROCEDURE

The conductance of Cu(001) thin films is determined using first-principles NEGF-DFT calculations as implemented in the SIESTA package [46]. The simulated system is a two-terminal device consisting of two electrodes that are semi-infinite along the Cu [100] transport direction (x axis) and are separated by a scattering region between the electrodes. Both electrodes and the scattering region form a thin film which is infinite along the [010] direction (y axis) but has a finite thickness of 6 to 12 monolayers (ML) along the z axis, corresponding to $d = 1 - 2$ nm using a fixed lattice constant $a = 0.3615$ nm. This is implemented using periodic boundary conditions and supercells with a constant width w of $3a$ along [010] to form a continuous film. This width corresponds to six atomic planes and was chosen to render effects due to the periodicity of frozen phonons and surface roughness negligible (<1% effect on electron transmission) and, more importantly, to create a large number of surface sites to reduce variations associated with the random surface roughness as described below. The supercells have a fixed height (along the z direction) of $10a$, so that the Cu only occupies a fraction of the cell while a vacuum of at least $4a$ is placed above/below the Cu, forming open Cu(001) surfaces. The length L of the scattering region along the transport direction (x axis) is varied from 1 to $10a$, which ultimately allows us to determine the resistivity from the length dependence of the calculated resistance. Each electrode is $1.5a$ long along the transport direction, corresponding to 3 MLs. Therefore, the total size of the simulated cell is $(L + 2 \times 1.5a) \times 3a \times 10a$.

The electronic structure is calculated with a Γ-centered $12 \times 6 \times 1\,k$-point mesh for the electrodes and a $1 \times 6 \times 1$ mesh for the scattering region. All calculations use a single-zeta basis with polarization orbitals [47,48], an energy shift of 0.02 Ry, a norm-conserving pseudopotential for copper that includes all core electrons up to the $3p$ electrons, and the Perdew-Burke-Ernzerhof (PBE) exchange correlation functional [49,50]. Electron smearing is carried out with a Fermi-Dirac occupation function with a temperature of 100 K. The electronic transport properties are then calculated using the TRANSIESTA [51] code with zero bias. Green's functions are determined with 32 points on the complex contour. The transmission coefficients are calculated with a $1 \times 255 \times 1\,k$-point mesh. Convergence tests as a function of all of these parameters indicate a numerical computational accuracy of ±1% for the calculated resistance values. We note that many simulated quantities in this study have considerably larger relative uncertainties, as indicated by the error bars. The primary reasons for this are that (i) the resistivity is effectively determined from the *difference* of two resistance values of similar size, which leads to a larger relative error, and (ii) average values from ensembles of simulated random configurations have standard deviations that are considerably larger than 1%.

Atomic-level surface roughness is introduced to the scattering region by randomly removing 50% of the atoms in both the top and bottom ML of the simulated film. Correspondingly, a simulation cell with for example $L = 5a$ has 60 surface atoms of which 30 are removed, since the two surfaces have an area of $5 \times 3a^2$ each and the (001) surface of an fcc crystal has two atoms per a^2. This corresponds to a reduction of the average film thickness by exactly one monolayer. That is, a simulation that starts out with, for example, a thickness of 6 ML (=$3a$) has a scattering region thickness $d = 5$ ML $= 2.5a =$ 0.90 nm after removal of the surface atoms. In contrast, the electrodes in this example still have a thickness of 6 ML and are therefore thicker than the scattering region. For any given set of scattering region length $L = 1 - 10\ a$ and layer thickness $d = 0.90-1.99$ nm, the resistance R is calculated using an ensemble of six to sixteen configurations of surface atoms that are randomly placed on surface lattice sites using a random number generator. These surface atoms are not relaxed, since their primary purpose is to cause electron scattering without representing a realistic surface morphology. The average R from these 6–16 calculations is subsequently used for further analysis and determination of the resistivity, while the standard deviation, which ranges in these calculations from 0.1% for $d = 1.99$ nm and $L = a$ to 5% for $d = 0.90$ nm and $L = 5a$, is taken as the statistical uncertainty of a given $R(L,d)$ value.

Frozen phonons are introduced in the scattering region in order to simulate systems which exhibit bulk electron scattering in addition to surface scattering. The idea of the frozen-phonon approach is that the fast-moving electrons only see a snapshot of the vibrating atoms [44,45]. Correspondingly, electron transport is calculated for configurations with fixed atomic positions which are, however, displaced from the equilibrium lattice sites to simulate the temperature-induced atomic vibrations. One direct approach to create an appropriate set of atomic displacements is to superpose all allowed modes and generate one corresponding configuration [52,53],

while another approach employs repeated calculations over an ensemble of systems in order to account for thermodynamic fluctuations [38], where each system exhibits different random displacements which are determined by molecular dynamics [38] or a chosen spatial distribution function [37,54]. In this work, we displace both bulk and surface atoms in the scattering region from their equilibrium position by a vector $\mathbf{\Delta}$, which is randomly determined for each atom by independently choosing its x, y, and z coordinates from a uniform distribution $U[-A,A]$, where A corresponds to the maximum amplitude of a local one-dimensional vibration. The temperature that corresponds to a particular A is determined by calculating the change in the potential energy vs displacement of one atom in a bulk supercell and setting the average potential energy corresponding to the uniform displacement distribution equal to $\frac{1}{2}kT$ per degree of freedom. That is, phonons are assumed to be local classical harmonic oscillators corresponding to the "Einstein model" for lattice vibrations. We note that surface atoms are expected to experience smaller force constants than bulk atoms and would therefore need to be displaced by a larger amplitude. This effect is neglected in this study because surface atoms are already very strongly disordered and therefore the vibration of them is expected to have a negligible effect on the overall resistance. The chosen approach of displacing atoms independently of each other has the advantage that the resulting frozen phonons are independent of the system size, that is, the scattering region size. In contrast, a physically more realistic model where phonons are displacement waves within the crystal would not only be computationally more demanding but also would lead to problems in interpreting the R vs L data which would no longer directly correspond to the resistivity but would also be affected by the changing system size as the phonons would be dependent on L. To validate this chosen frozen-phonon approach, bulk transport simulations that include frozen phonons but no surfaces were done by NEGF-DFT, using a two terminal configuration with a variable-length scattering region. These calculations employ the same computational parameters as those used for the thin-film calculations, except there is no vacuum in the supercell, the cross-sectional area of the supercell perpendicular to the transport direction is $2a \times 2a$, and k-point meshes are $12 \times 6 \times 6$ and $1 \times 6 \times 6$ for the electrodes and scattering region, respectively, and $1 \times 255 \times 255$ for the transport calculation.

III. RESULTS

We first present results from bulk transport simulations that are used to validate the frozen-phonon approach and the system temperature. For these calculations, all atoms within the scattering region are randomly and individually displaced following a uniform distribution with a maximum amplitude A in each dimension, as described in more detail in the previous section. Figure 1(a) is a plot of the calculated resistance R as a function of the length L of the scattering region, where $L = 3-6$ is given in units of the lattice constant $a = 3.615$Å, yielding $L = 1.08-2.17$ nm. The simulated system cell has a cross-sectional area of $2a \times 2a$, such that the scattering region contains a total of 48–96 atoms. Calculations are done for maximum displacements $A = 0$, $0.02a$, $0.03a$, $0.04a$, $0.05a$, and $0.06a$, which are equal to atomic displacements

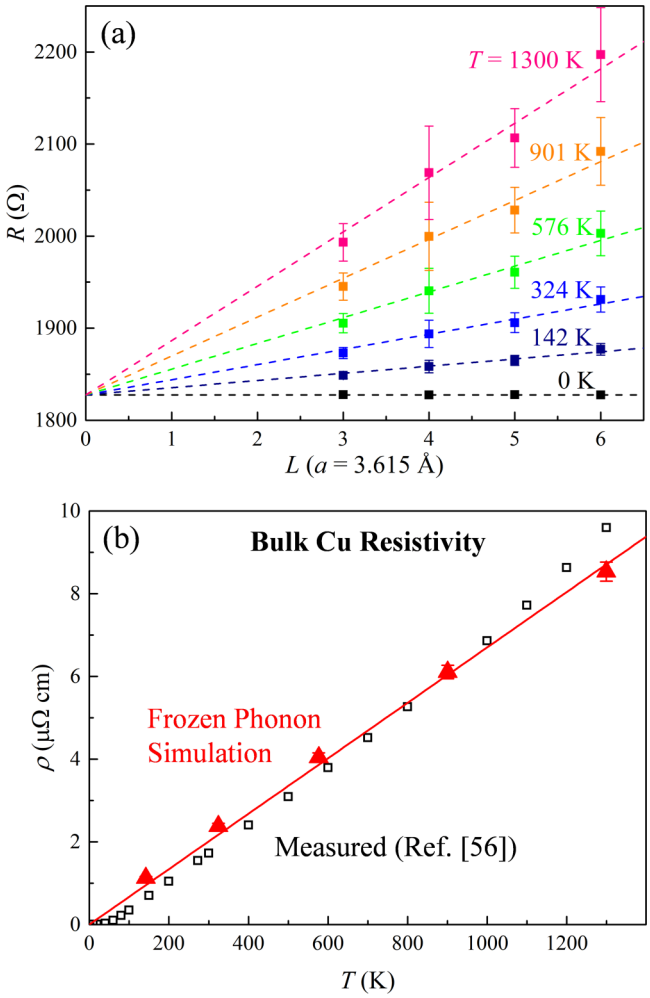

FIG. 1. (a) Calculated resistance R vs length L of simulated scattering region for bulk Cu with frozen phonons corresponding to temperatures $T = 0-1300$ K. (b) Bulk resistivity ρ vs T, as determined from the slopes in (a) (red triangles). The black open squares indicate the experimental Cu bulk resistivity from Ref. [56].

of 0−0.22Å and correspond to classical temperatures of 0, 142, 324, 576, 901, and 1300 K, respectively. The resistance at $T = 0$ K is 1828 Ω and is independent of L. This is expected since this resistance corresponds to the ballistic resistance R_0 which is independent of conductor length. The calculated values for the four different $L = 3$, 4, 5, and 6 a vary by only 0.005%, indicating a negligible numerical variation associated with the unit cell length. The specific ballistic resistance $R_0(wd) = 0.955 \times 10^{-15}$ Ω m^2 is within the range $0.91 - 1.01 \times 10^{-15}$ Ω m^2 of previously reported values for the ballistic resistance of Cu along the [100] direction [13,39,55].

In contrast, the data labeled with $T = 142$ K in Fig. 1(a) indicate resistances that are larger than R_0 and increase with increasing L. Each data point corresponds to the average R of four separate calculations with different random atomic displacements with an amplitude $A = 0.02a$, while the plotted error bar indicates the standard deviation from these four calculations. R increases linearly with L, as indicated with the line through the data points which is the result from a linear

fit that is forced to go through R_0 at $L = 0$. That is, the only fitting parameter is the R-vs-L slope, which corresponds to the resistivity $\rho = 1.13 \pm 0.03\ \mu\Omega$ cm due to the frozen phonons at $T = 142$ K. Similarly, the data for $T = 324 - 1300$ K also exhibit linear $R(L)$ relationships, suggesting a well-defined resistivity associated with the frozen phonons [38]. The plotted error bars increase with increasing T. This is attributed to the increasing displacement amplitudes which lead to larger variations in the random displacement configurations.

Figure 1(b) is a plot of the resistivity ρ vs temperature T, as determined from the slopes in Fig. 1(a). It increases approximately linearly from $1.13 \pm 0.03\ \mu\Omega$ cm for $T = 142$ to 2.38 ± 0.07, 4.04 ± 0.11, 6.11 ± 0.16, and $8.53 \pm 0.23\ \mu\Omega$ cm for $T = 324$, 576, 901, and 1300 K. The linear relationship is also indicated by the solid line from linear fitting of the data points forced through the origin. Figure 1(b) also shows as open symbols the known experimentally measured resistivity of copper from Ref. [56]. Our frozen-phonon calculations are in good agreement with the experimental resistivity, with deviations of $<13\%$ for $T = 400-1000$ K. The calculations overestimate ρ at low temperature, by 76% and 26% for $T = 142$ and 324 K, respectively, which is expected because the simulated phonons are purely classical and, therefore, their density is proportional to T, while quantization in true solids leads to a stronger-than-linear decrease in the phonon density as their energy becomes comparable to or smaller than kT. The low-temperature resistivity can be correctly predicted by calculating and populating the eigenvalues of collective lattice vibrations (i.e., phonon modes), as shown by Liu *et al.* [52]. This approach is not used here, because we are primarily interested in high temperatures and, more importantly, our approach has the advantage of a phonon population that is completely independent of the length of the scattering region, as described in the previous section. Also, Fig. 1(b) shows that the experimental resistivity increases more steeply as the temperature approaches the Cu melting point $T_m = 1358$ K. We attribute this to additional electron scattering at Cu vacancies, which have a density of 0.76×10^{-3} per lattice site at T_m [57].

For the remainder of this paper, we explore the effect of phonons on electron transport using a single displacement amplitude $A = 0.0498a$ that corresponds to a nominal temperature $T = 900$ K. For this temperature, the simulated resistivity agrees with experiment within 1%. We note that it is also possible to perform low-temperature simulations using our frozen-phonon approach. In that case, the A vs T relationship would need to be more carefully done, likely by calibrating the temperature with the experimental resistivity. We emphasize here again that the data in Fig. 1(b) represent a true first-principles prediction of the temperature dependence of the resistivity of Cu using a rather simple frozen-phonon approach that, however, leads to an accurate resistivity prediction at medium to high temperatures. Thus, in summary, we conclude that the chosen frozen-phonon approach is well suited to cause temperature-induced electron bulk scattering in our transport simulations and is used in the following simulations of Cu(001) thin films.

Figure 2 shows the results from transport simulations on Cu(001) thin films with thickness $d = 0.90-1.99$ nm at $T = 0$ and 900 K. The resistance R is calculated as a function of the length L of the scattering region for simulated cells that are $w = 3a = 1.08$ nm wide and are terminated by periodic boundary conditions on their sides to effectively simulate an infinitely wide thin film, as described in more detail in Sec. II. Figure 2(a) is a schematic that illustrates the simulated geometry. For each configuration, the surface atoms in the scattering region are randomly placed on 50% of lattice sites and, for $T = 900$ K,

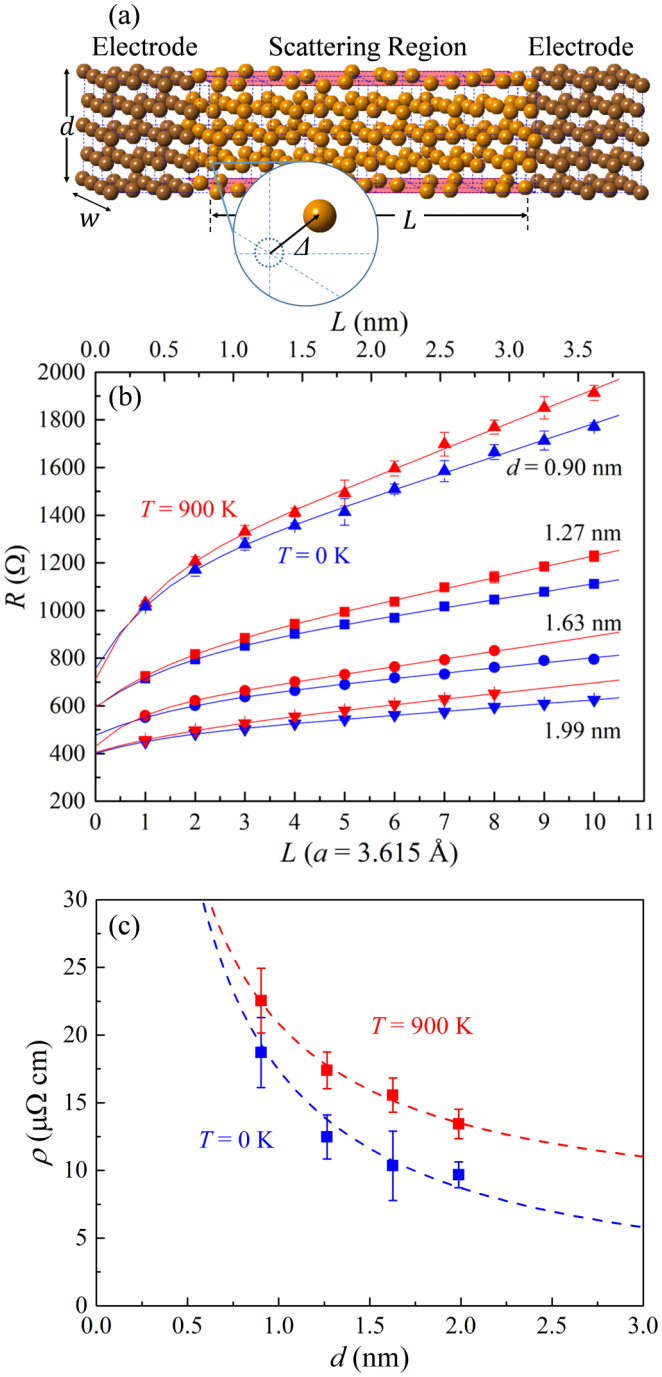

FIG. 2. (a) Schematic of the simulated system including a scattering region with 50% of surface vacancies and random atomic displacements Δ, causing surface and phonon scattering, respectively. (b) Calculated resistance R vs length L and (c) resistivity ρ vs thickness d of Cu(001) thin films at temperatures $T = 0$ and 900 K. The dashed lines in (c) are from curve fitting using Eq. (8).

the atoms in the scattering region are also displaced by a random $\mathbf{\Delta}$ from their lattice site to form frozen phonons as described in detail in the previous section. The plot in Fig. 2(b) shows a total of 76 data points, each representing the average R from a minimum of six calculated configurations. The data set for $d = 0.90$ nm and $T = 0$ K is from a 5-ML-thick layer. Its resistance increases monotonically from $R = 1017 \pm 5\,\Omega$ for $L = 0.3615$ nm to $R = 1772 \pm 17\,\mu\Omega$ cm for $L = 3.615$ nm, which is attributed to electron scattering at the atomically rough surfaces. The increase is steep for small L but the slope approaches relatively quickly a constant value, as illustrated by the line through the data points in Fig. 2(b) which is approximately straight for $L > 4a$. This line is obtained from data fitting using $R = R_0 + mL - \alpha e^{-\beta L}$, where R_0 is the ballistic resistance, m is the slope at large L which defines the resistivity due to surface scattering, and the last term is an exponential decay that accounts for the nonlinearity at small L which is attributed to a tunneling current between the two electrodes that lowers the overall resistance. Fitting yields $R_0 = 1095\,\Omega$, which is slightly larger than the calculated ballistic resistance of 1021 Ω for a smooth copper layer with the same thickness (5 ML) and width, indicating an increase in the ballistic resistance due to the rough surfaces, consistent with an earlier report on the decrease in the ballistic conductance of Cu layers with periodic surface roughness [36]. Extrapolating the fitted line to zero length yields $R(L = 0) = R_0 - \alpha = 1095\,\Omega - 338\,\Omega = 757\,\Omega$, which is slightly smaller than the calculated ballistic resistance of 856 Ω for the 6-ML-thick electrodes, indicating a relatively large uncertainty (as expected) in extrapolating an exponential function. The inverse of β is the decay length of the exponential tail for electrode-electrode tunneling and is sufficiently small ($1.2a$) such that the correction to the resistance due to the tunneling becomes negligible (<0.5%) for $L > 5a$. This confirms a good linearity with a well-defined slope m that is unaffected by the uncertainty in the exact fit of the exponential tail. m is used to determine the resistivity $\rho = m(wd)$.

This fitting process is repeated for different thicknesses and temperatures, as indicated by the lines in Fig. 2(b). For $T = 0$ K, the ballistic resistance decreases from $R_0 = 1095$ to 784, 590, and 463 Ω, as d increases from 0.90 to 1.27, 1.63 to 1.99 nm, respectively, showing an expected proportionality between ballistic resistance and the inverse of cross-sectional area. The slope m, however, decreases much faster, from 69 to 32.9, 21.2, and $16.2\,\Omega/a$, indicating a strong thickness dependence of layer resistivity, which is caused by surface scattering. The data for $T = 900$ K exhibit a comparable thickness dependence but steeper slopes for all d, which is attributed to the additional phonon scattering resistivity. In contrast, the ballistic resistances $R_0 = 1097$, 772, 573, and 472 Ω for $T = 900$ K are nearly identical to the $T = 0$ K values, which is expected since bulk scattering does not contribute to the ballistic resistance (contact resistance).

Figure 2(c) shows the resistivity from all eight data sets, that is, for four thicknesses $d = 0.90$, 1.27, 1.63, and 1.99 nm and two temperatures $T = 0$ and 900 K. The values are determined from the slopes m of the fitted curves in Fig. 2(b), and the dashed lines through the data points in Fig. 2(c) are from curve fitting using Eq. (8), as discussed in Sec. IV. The zero-temperature ρ increases with decreasing d, from 9.7 ± 1.0 to 10.4 ± 2.6, 12.5 ± 1.6, and $18.7 \pm 2.6\,\mu\Omega$ cm. This resistivity is purely due to surface scattering and is in direct contradiction to the classical F-S model, which predicts a zero resistivity in the absence of bulk (phonon and/or defect) scattering [1,2]. As discussed in Sec. I, we attribute this discrepancy to a limitation of the F-S model, where carriers that move parallel to the surface never interact with the surfaces and therefore have, in the absence of bulk scattering, a diverging (infinite) contribution to the conductance. The resistivity at $T = 900$ K similarly increases with decreasing d, from 13.4 ± 1.1 to 15.6 ± 1.3, 17.4 ± 1.4, and $22.5 \pm 2.4\,\mu\Omega$ cm. These values are all larger than those for $T = 0$ K, which is attributed to additional electron scattering at the frozen phonons. The resistivity difference between 0 and 900 K is $\Delta\rho_{ph} = 3.7 \pm 1.5$, 5.2 ± 2.9, 4.9 ± 2.1, and $3.8 \pm 3.5\,\mu\Omega$ cm, respectively. These values are relatively independent of layer thickness despite that d varies by more than a factor of two from $d = 0.90$ to 1.99. This suggests that, within the large numerical uncertainty, the resistivity contributions from phonon and surface scattering are additive, such that no deviation from Matthiessen's rule can be detected. To explore the effect of phonon scattering in thin films further, the resistivity at 900 K of smooth thin films with frozen phonons was calculated by determining the slope of R vs L similarly to what was done in Fig. 2, but without surface roughness. This provides values $\Delta\rho_{ph} = 6.06 \pm 0.14$, 5.48 ± 0.13, 5.81 ± 0.14, and $5.81 \pm 0.05\,\mu\Omega$ cm for smooth layers with $d = 1.08$, 1.45, 1.81, and 2.17 nm, yielding an average of $5.8 \pm 0.1\,\mu\Omega$ cm. This is close to the calculated bulk resistivity at 900 K of $6.11 \pm 0.16\,\mu\Omega$ cm, but is larger than the average $\Delta\rho_{ph} = 4.4 \pm 1.3\,\mu\Omega$ cm for the rough layers. That is, the resistivity contribution due to phonon scattering is the same for bulk and flat thin film calculations, but is smaller for the rough films. Correspondingly, we conclude that (i) the change in the electronic structure from bulk to thin film has a negligible effect on the electron-phonon scattering for our 1–2 nm thick Cu(001) layers and (ii) there is a deviation from Matthiessen's rule for electron scattering at surfaces and phonons. The latter may be attributed to the fact that electrons that scatter at the potential variation of the rough surface will not scatter more strongly if the surface atom is also displaced by a frozen phonon. Thus, the large fraction of atoms that are at the surface in our thin films effectively reduce the phonon contribution to the resistivity $\Delta\rho_{ph}$ for thin films with roughness. We note though that the difference between $\Delta\rho_{ph} = 4.4 \pm 1.3\,\mu\Omega$ cm from rough layers and $5.8 \pm 0.1\,\mu\Omega$ cm from smooth films is of similar magnitude to that of the computational accuracy, such that the data do not unequivocally demonstrate a deviation from Matthiessen's rule.

IV. DISCUSSION

This section discusses possible functional forms of the resistivity size effect of thin films. That is, it explores whether physical models that predict a ρ vs d dependency are consistent with the computational results presented in Sec. III. For this purpose, we first compare the prediction of the classical Fuchs-Sondheimer model with the calculated data, followed by a discussion of a classical 2D transport model, quantum models, and a generic power-law fitting of the data.

A. Fuchs-Sondheimer model

The classical F-S model employs Boltzmann transport equations to derive an explicit expression for the thin-film resistivity [1,2]

$$\rho = \rho_0\left[1 - \frac{3}{2\kappa}(1-p)\int_1^\infty \left(\frac{1}{t^3} - \frac{1}{t^5}\right)\frac{1-e^{-\kappa t}}{1-pe^{-\kappa t}}dt\right]^{-1}, \quad (1)$$

where ρ_0 is the bulk resistivity that quantifies electron relaxation due to bulk (phonon) scattering, $\kappa = d/\lambda$, and the phenomenological specularity parameter p defines the fraction of electrons which retain their in-plane momentum when reflecting off the surface, as accounted for as a boundary condition. That is, $p = 0$ and 1 correspond to diffuse and specular surface scattering, respectively, while the parameter κ defines the relative importance of bulk vs surface scattering. More specifically, $\kappa \to \infty$ represents the bulk scattering dominated regime at relatively large thickness and/or high temperature, leading to a well-known approximate F-S formula $\rho = \rho_0[1 + 3\lambda(1-p)/8d]$ that deviates by only 9% from Eq. (1) for $0.05 < \kappa < 1$, and converges to Eq. (1) for increasing $\kappa > 1$ [33,58]. This approximate form implies that surface scattering results in an additive resistivity term that is proportional to $1/d$, as often reported from experiments [27,30,59]. In contrast, $\kappa \to 0$ represents the surface scattering dominated regime at small thickness and/or low temperature, where Eq. (1) converges to $\rho = 4\rho_0\lambda(1-p)/[3(1+p)d\ln(\lambda/d)]$ [1,2]. That is, ρ is proportional to $1/[d\ln(\lambda/d)]$ and, since the product $\rho_0 \times \lambda$ is independent of temperature [60], the limit of vanishing bulk scattering ($\lambda \to \infty$) leads to a vanishing thin-film resistivity [3]. This limitation is illustrated in Fig. 3(a).

Figure 3(a) is a plot of the calculated Cu(001) thin-film resistivity together with curves obtained from data fitting using the F-S model in Eq. (1). The data points are identical to what is shown in Fig. 2(c), but are plotted vs the inverse of thickness such that the bulk values $\rho_0 = 0$ and 6.1 $\mu\Omega$ cm at 0 and 900 K, respectively, can be directly plotted at $1/d = 0$, representing the important limit of thick ($d \to \infty$) layers. The plotted line fits the data well for $T = 900$ K. It is obtained using the known product $\rho_0 \times \lambda = 6.7 \times 10^{-16}$ Ωm^2 which corresponds to a room-temperature $\rho_0 = 1.678\,\mu\Omega$ cm and $\lambda = 39.9$ nm [60]. Correspondingly, the only fitting parameter is the surface scattering specularity which was found to be $p = 0.37$, suggesting that the simulated surface roughness represented by a random 50% occupation of a surface monolayer causes 37% of electrons to scatter specularly, while correspondingly 63% of surface scattering is diffuse. That is, the relatively rough simulated surface causes more diffuse scattering than experimental smooth Cu(001) surfaces with a reported specularity $p = 0.67$ [31]. The red dashed line in Fig. 3(a) has a slight negative curvature, since the predicted increase in ρ from Eq. (1) is less than for a linear ρ vs $1/d$ relationship. A straight line would be expected for the large-thickness high-temperature limit of the approximate F-S model which, however, is not perfectly applicable because $T = 900$ K and $d > 0.90$ nm corresponds to a relatively small $\kappa > 0.08$. We note that the plotted data points would be better described by a straight line than the plotted F-S prediction.

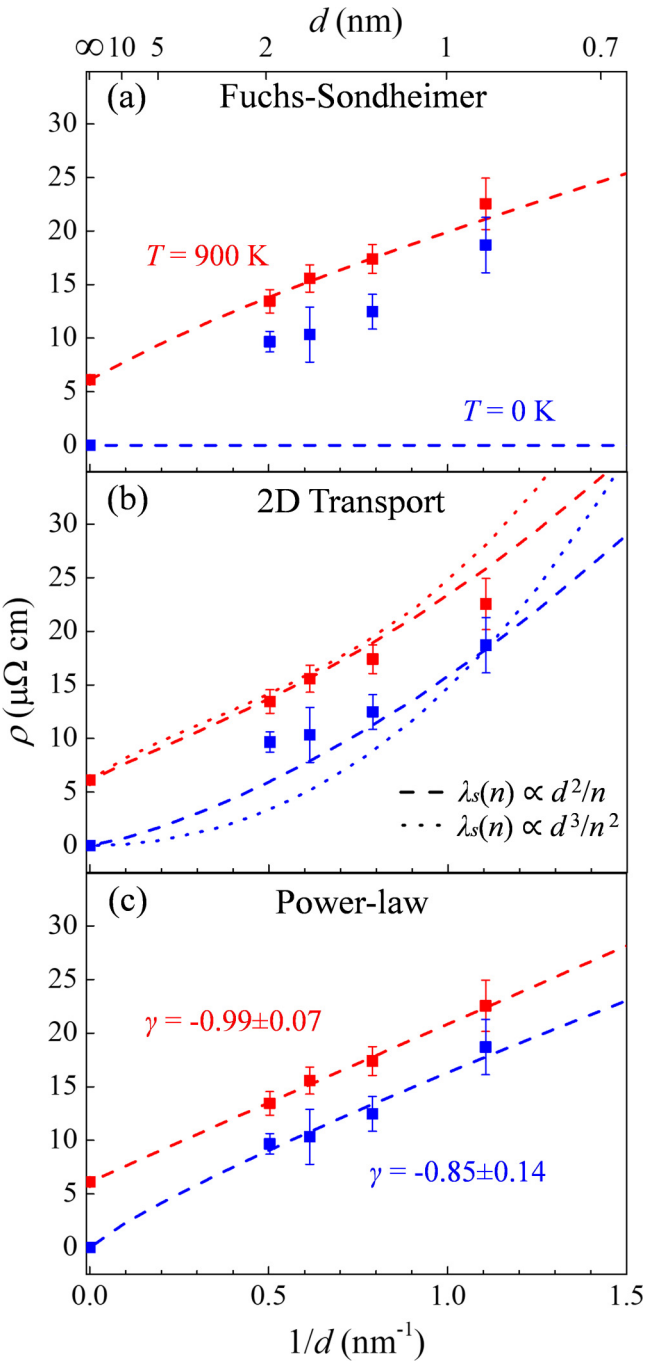

FIG. 3. The simulated resistivity ρ vs the inverse of the thickness d of Cu(001) layers at 0 and 900 K. The curves are from data fitting using (a) the Fuchs-Sondheimer model according to Eq. (1), (b) 2D semiclassical (dashed line) and quantum transport (dotted line) models according to Eqs. (4) and (5), and (c) a power law according to Eq. (7).

This apparent linear increase in ρ vs $1/d$ is further discussed below in subsection D.

In contrast, for $T = 0$ K and no bulk-defect scattering, the F-S model predicts a thickness-independent $\rho = 0\,\mu\Omega$ cm, regardless of the choice of fitting parameters. This is represented in Fig. 3(a) with the horizontal line which completely fails to describe the calculated zero-temperature thin-film resistivity.

We attribute this breakdown to an intrinsic limitation of the F-S model, which does not include any electron relaxation due to surface scattering. Correspondingly, in the limit of $\rho_0 \to 0$, the F-S prediction of the thin-film resistivity also vanishes which is in complete contradiction with our calculated $T = 0$ K data.

B. Semiclassical 2D transport

Two-dimensional (2D) transport models avoid the low-temperature breakdown of the F-S model. This is achieved by electron surface scattering which causes electron relaxation and is quantified by a surface-scattering mean-free path λ_s. In this framework, the electrons are confined between the surfaces of a thin film, forming a standing wave $\varphi_n = \sqrt{2/d}\sin(n\pi z/d)$ perpendicular to the surface. This gives rise to multiple conduction channels with a subband index n and quantized wave vectors $k_z = n\pi/d$ perpendicular to the layer surface [5,61]. At small thickness, this electronic structure is very different from that of the bulk, and the total in-plane conductivity σ is obtained from the sum over all channels [5]. Following this approach, we express the conductivity of a thin film as

$$\sigma = \frac{e^2}{h}\frac{1}{k_F d}\sum_{n=1}^{N_c} k_{\mathrm{II}}^2 \left(\frac{1}{\lambda} + \frac{1}{\lambda_s(n)}\right)^{-1}, \tag{2}$$

where k_F is the length of the 3D Fermi vector which itself depends on the thickness d, $k_{\mathrm{II}} = \sqrt{k_F^2 - k_z^2} = \sqrt{k_F^2 - n^2\pi^2/d^2}$ is the n-dependent length of the wave vector component within the plane of the film, $N_c \approx k_F d/\pi$ is the total number of channels, and $\lambda_s(n)$ is the electron mean-free path due to surface scattering, which is thickness and channel dependent and defined in three-dimensional space in order to be compatible with the bulk mean-free path λ. Equation (2) can be used within a semiclassical description for transport in thin films. In that case, the distance that is traveled by an electron between the two surfaces is $d \times k_F/k_z$, and correspondingly, the classical mean-free path for surface scattering becomes

$$\lambda_s(n) = \frac{k_F d}{k_z(1-p)} = \frac{k_F d^2}{n\pi(1-p)}. \tag{3}$$

This expression can now directly be used in Eq. (2), yielding the thin-film resistivity within the framework of a semiclassical 2D conductor:

$$\rho = \frac{h}{\lambda e^2 d}\left[\sum_{n=1}^{N_c} \frac{k_F^2 - n^2\pi^2/d^2}{k_F d^2 + n\pi\lambda(1-p)}\right]^{-1}. \tag{4}$$

We note that for the limiting case of large thickness ($d/\lambda \to \infty$), Eq. (4) converges to the approximate F-S formula $\rho = \rho_0[1 + 3\lambda(1-p)/8d]$ where $\rho_0 = (3\pi h)/(2e^2 {k_F}^2 \lambda)$. This holds true as long as $N_c \approx k_F d/\pi \gg 1$. That is, the 2D semiclassical model prediction in Eq. (4) converges for the bulk scattering dominated regime ($\kappa \to \infty$) to the F-S model if $d \gg \pi/k_F$, which corresponds for the case of copper to $d \gg 0.23$ nm. Additionally, the prediction for ρ in Eq. (4) does not vanish in the zero-temperature ($\lambda \to \infty$) limit, correcting the problematic prediction of the F-S model in the surface scattering dominated ($\kappa \to 0$) regime.

The dashed lines in Fig. 3(b) show the result from data fitting using the 2D semiclassical expression in Eq. (4). This is done by numerical summation over all channels where the only free fitting parameter is the specularity parameter p, which is expected to be temperature-independent. Correspondingly, fitting is done simultaneously for both temperatures, yielding $p = 0.35$. This is close to the value $p = 0.37$ obtained using the F-S model, as described above. The curves do not satisfactorily describe the simulated data points and suggest a considerably stronger resistivity scaling. More specifically, the plotted curves exhibit a stronger curvature than the data points and underestimate the resistivity at low temperature and large thickness, but overestimate the resistivity at high temperature and small thickness. Nevertheless, this 2D semiclassical model provides a clear improvement over the F-S model for the zero-temperature limit [horizontal line in Fig. 3(a)]. This is attributed to two key improvements, namely (i) describing electrons as quantized standing waves in the perpendicular space, and (ii) introducing a mean-free path for surface scattering.

C. Quantum models

Full quantum mechanical approaches have also been applied to study electron-surface scattering in thin films [3,4,5,7]. In these models, the electron conductivity is predicted as a function of the electronic potential and the geometry of the surface roughness, treating the surface roughness as a perturbation to the flat surfaces' Hamiltonian. For the case of small roughness, studies by Calecki [5], Tešanović *et al.* [3], Trivedi *et al.* [4], and Sheng *et al.* [7] all predict a channel-dependent mean-free path in the surface-dominated regime that is proportional to the cube of the thickness, i.e., $\lambda_s(n) \propto d^3/n^2$, which results in a resistivity contribution from the surface that increases with the inverse square of the thickness: $(\rho - \rho_0) \propto 1/d^2$. Without replicating the details of these quantum model approaches, their result can be qualitatively understood by examining the electron wave near the surface: The scattering probability $1/\tau_s$ is proportional to $\langle\varphi_n|V(z)|\varphi_n\rangle = \int V(z)(2/d)\sin^2(n\pi/d)dz$, where $V(z)$ is the scattering potential. Since $V(z)$ is localized at the surface, $1/\tau_s \propto \int V(z)(2/d)(n\pi/d)^2 dz \propto n^2/d^3$. Accordingly, the thin-film resistivity in the surface-dominated regime was derived by Sheng *et al.* [7] for the case of small roughness:

$$\rho = \frac{hk_F d}{e^2}\left[\sum_{n=1}^{N_c} \frac{k_F^2 - n^2\pi^2/d^2}{\lambda^{-1} + 4n^2\pi^2 Q_0/(k_F d^3)}\right]^{-1}, \tag{5}$$

where Q_0 quantifies the effect from the surface morphology. This expression implies an effective mean-free path due to surface scattering of

$$\lambda_s(n) = \frac{k_F d^3}{4n^2\pi^2 Q_0}. \tag{6}$$

We note, Eq. (5) converges to the F-S prediction in the limit $\kappa \to \infty$, defining the relationship between the roughness factor Q_0 and the specularity parameter p, as $Q_0 = 15(1-p)/(32k_F)$.

The dotted lines in Fig. 3(b) are from fitting the data using the expression in Eq. (5), which is done by numerical determination of the sum as a function of d, while keeping the fitting parameter Q_0 the same for the two temperatures. However, the curves do not well describe the calculated data points. More specifically, the predicted resistivity from this model increases

too steeply with decreasing d. We note that the model also fails at large thickness, since the $Q_0 = 0.037$ nm from the fitting procedure corresponds to an unphysical specularity parameter $p = -0.1$, slightly outside the allowed range $0 \leqslant p \leqslant 1$.

We attribute the failure of the quantum models to the small-roughness approximation. This approximation requires that (i) the lateral correlation length is small in comparison to the Fermi wavelength which effectively means that the maximum surface mound width is comparable to the size of atoms. This requirement is met for our simulations, since the random atomic surface roughness has a characteristic scale of one atom. However, more generally, this requirement is not satisfied in realistic thin films with mound features with typical lateral length scales of 2–100 nm, resulting in an additional roughness term to the resistivity [13,19]. We note that this correction has been directly included in some quantum models which predict a resistivity scaling that is more complex than $1/d^2$ for the case of long-range correlated surfaces [4,7]. Second, the small-roughness approximation requires that (ii) the root-mean-square roughness is small compared to the film thickness [3,4,5,7]. This requirement is not met in our simulations since the surface monolayers that define the roughness represent a considerable fraction of the overall layer thickness. For example, the thinnest simulated layer has just four perfect Cu monolayers between the two surface roughness monolayers. Consistent with this argument, a recent report on transport in Cu suggests that electron transmission is severely degraded near the surface, approximately ∼0.5 nm deep into the film [41], which corresponds to the entire simulated layer with two surfaces for $d < 1$ nm. Correspondingly, the predicted $1/d^2$ proportionality from the proposed quantum models for the resistivity contribution in the thin-layer limit does not apply to our simulation results. We also note that the quantum models assume well-defined channels which may not correctly account for channel mixing associated with the strong disorder at the surface.

D. Power law

In an attempt to determine a functional form that satisfactorily describes the resistivity vs thickness data from our simulations, we use a general power-law expression for the thin-film resistivity

$$\rho = \rho_0 + f d^{\gamma}. \tag{7}$$

The prefactor f and exponent γ are functions of ρ_0. That is, they are not assumed to be temperature-independent, so that Matthiessen's rule is not pre-assumed, consistent with the discussion in Sec. III. Figure 3(c) shows the result from the power-law fitting with Eq. (7). The plotted curves describe the data points well—considerably better than the alternative models presented in Figs. 3(a) and 3(b). The fitting procedure provides values for γ of -0.85 ± 0.14 at 0 K and -0.99 ± 0.07 at 900 K. That is, considering the computational uncertainty, the exponent is -1 for both temperatures, implying an inverse thickness dependence for the resistivity contribution from surface scattering. This is in good agreement with previous work by Ke *et al.* [43] and Zahid *et al.* [15], who reported surface scattering resistivity values calculated with nonequilibrium DFT methods including vertex correction [62], and used the approximate F-S formula with a $1/d$ dependence to describe their data. Based on the $1/d$ dependence for the resistivity contribution due to surface scattering at both 0 and 900 K, we assume that the $1/d$ dependence is also valid for any other temperature between 0 and 900 K. In that case, Eq. (2) can only be satisfied if $\lambda_s(n)$ is channel-independent and proportional to d. This implies that the surface scattering probability is independent of the channel, which means independent of the momentum perpendicular to the surface and/or the probability distribution (i.e., the square of the wave function) of the electron within the conducting film. This is clearly different from the assumptions for the quantum models described above, and suggests a surface scattering that is "bulklike." That is, opposite to the above models, surface scattering does not only occur at the physical surface but extends into the film. We attribute this to the simulated films consisting of only a few monolayers, such that the perturbation of the electron potential by the surface roughness extends throughout the thickness of the layer, causing scattering of electrons even if they have wave functions that vanish near the surface.

Correspondingly, based on this temperature-independent $1/d$ dependence of the resistivity contribution due to surface scattering, Eq. (7) with a fixed $\gamma = -1$ yields an expression for the thin-film resistivity ρ with a surface-scattering mean-free path λ_s that is proportional to the thickness d and both temperature-independent and channel-independent:

$$\rho = \rho_0\left(1 + \frac{\lambda}{\lambda_s}\right), \quad \lambda_s = \alpha \times d. \tag{8}$$

The proportionality constant α is independent of temperature and thickness and is a function of the electronic structure of the surface. We use Eq. (8) for data fitting of the simulated resistivity, plotted as dashed lines in Fig. 2(c). The curves describe the plotted data relatively well and yield $\lambda_s = (3.8 \pm 0.2) \times d$ and $(4.4 \pm 0.1) \times d$ at $T = 0$ and 900 K, respectively. That is, the mean-free path associated with electron scattering at the simulated monolayer roughness is only four times the layer thickness. Correspondingly, electron surface scattering is expected to dominate the resistivity for layers that are at least four times thinner than the bulk mean-free path λ. This corresponds to a critical thickness of 10 nm for Cu at room temperature below which electron surface scattering dominates. We note that α for $T = 900$ K is 16% larger than for $T = 0$ K, which can be attributed to the uncertainty but may also indicate a trend towards larger λ_s with increasing T. Such an increase in λ_s with increasing T (or correspondingly decreasing λ) is consistent with the above discussion on the deviation from Matthiessen's rule. More specifically, an electron that scatters on a displaced atom (phonon) will not scatter "more" if this atom also belongs to a surface roughness. This effectively reduces the effect of electron surface scattering with increasing temperature, leading to an increase in λ_s.

We note that Eq. (8) proposes the same functional form as the approximate F-S model. However, based on the discussion above, Eq. (8) is valid for very thin layers for which surface scattering becomes bulklike while the approximate F-S model is valid in the limit of large thickness. More specifically, the simulations in this work suggest a resistivity contribution due to surface scattering on Cu(001) surfaces that is proportional

to $1/d$ for the simulated range $d = 1 - 2$ nm, while previous studies (including the classical F-S model) suggest the same $1/d$ dependence for approximately $d > 20$ nm [16,18,31,32]. It is not evident from our results whether the intermediate range, $d = 2-20$ nm, exhibits the same functional form.

V. CONCLUSIONS

First-principles simulations of electron transport in 1–2 nm thick Cu(001) layers with electron scattering at both surface roughness and bulk phonons suggest an additive resistivity term due to electron surface scattering that is nearly temperature-independent and inversely proportional to the thickness. The calculated thin-film resistivity at 0 K is finite, contradicting the classical F-S model prediction and indicating a breakdown of the F-S model in the surface scattering dominated regime. Both classical and quantum 2D transport models correct the problematic F-S prediction at zero temperature. However, they fail to correctly describe the $1/d$ dependence. This is attributed to the small-surface-roughness approximation in these models, which is not satisfied for the simulated layers. The surface scattering in the simulations is bulklike and described with a channel-independent mean-free path λ_s that is proportional to d, leading to the additive $1/d$ resistivity term. This functional form matches the approximate F-S prediction for the case of relatively thick layers. Therefore, the $1/d$ dependence is expected for both thin (<2 nm) and thick (>20 nm) layers, while the intermediate 2–20 nm range may yield another functional form.

ACKNOWLEDGMENTS

This research is funded by SRC, MARCO, and DARPA through the FAME STARnet center. The authors also acknowledge the NSF under Grant No. 1712752. Computational resources were provided by the Center for Computational Innovations at RPI.

[1] K. Fuchs, Math. Proc. Cambridge Philos. Soc. **34**, 100 (1938).
[2] E. H. Sondheimer, Adv. Phys. **1**, 1 (1952).
[3] Z. Tešanović, M. V. Jarić, and S. Maekawa, Phys. Rev. Lett. **57**, 2760 (1986).
[4] N. Trivedi and N. W. Ashcroft, Phys. Rev. B **38**, 12298 (1988).
[5] D. Calecki, Phys. Rev. B **42**, 6906 (1990).
[6] G. Fishman and D. Calecki, Phys. Rev. B **43**, 11581 (1991).
[7] L. Sheng, D. Y. Xing, and Z. D. Wang, Phys. Rev. B **51**, 7325 (1995).
[8] S. Chatterjee and A. E. Meyerovich, Phys. Rev. B **81**, 245409 (2010).
[9] K. Moors, B. Sorée, Z. Tőkei, and W. Magnus, J. Appl. Phys. **116**, 063714 (2014).
[10] K. Moors, B. Sorée, and W. Magnus, J. Appl. Phys. **118**, 124307 (2015).
[11] K. Moors, B. Sorée, and W. Magnus, Microelectron. Engieering **167**, 37 (2017).
[12] R. C. Munoz and C. Arenas, Appl. Phys. Rev. **4**, 011102 (2017).
[13] T. Zhou, P. Y. Zheng, S. C. Pandey, R. Sundararaman, and D. Gall, J. Appl. Phys. **123** (2018), doi: 10.1063/1.5020577.
[14] Y. P. Timalsina, A. Horning, R. F. Spivey, K. M. Lewis, T.-S. Kuan, G.-C. Wang, and T.-M. Lu, Nanotechnology **26**, 075704 (2015).
[15] F. Zahid, Y. Ke, D. Gall, and H. Guo, Phys. Rev. B **81**, 045406 (2010).
[16] P. Y. Zheng, R. P. Deng, and D. Gall, Appl. Phys. Lett. **105**, 131603 (2014).
[17] J. S. Chawla, F. Zahid, H. Guo, and D. Gall, Appl. Phys. Lett. **97**, 132106 (2010).
[18] H.-D. Liu, Y.-P. Zhao, G. Ramanath, S. P. Murarka, and G.-C. Wang, Thin Solid Films **384**, 151 (2001).
[19] P. Y. Zheng, T. Zhou, B. J. Engler, J. S. Chawla, R. Hull, and D. Gall, J. Appl. Phys. **122**, 095304 (2017).
[20] P. Zheng, T. Zhou, and D. Gall, Semicond. Sci. Technol. **31**, 055005 (2016).
[21] M. César, D. Gall, and H. Guo, Phys. Rev. Appl. **5**, 054018 (2016).
[22] D. Choi, X. Liu, P. K. Schelling, K. R. Coffey, and K. Barmak, J. Appl. Phys. **115**, 104308 (2014).
[23] Y. P. Timalsina, X. Shen, G. Boruchowitz, Z. Fu, G. Qian, M. Yamaguchi, G.-C. Wang, K. M. Lewis, and T.-M. Lu, Appl. Phys. Lett. **103**, 191602 (2013).
[24] J. M. Camacho and A. I. Oliva, Thin Solid Films **515**, 1881 (2006).
[25] S. Dutta, K. Sankaran, K. Moors, G. Pourtois, S. Van Elshocht, J. Bommels, W. Vandervorst, Z. Tokei, and C. Adelmann, J. Appl. Phys. **122**, 025107 (2017).
[26] R. Henriquez, V. Del, C. Gonzalez-Fuentes, J. Correa-Puerta, L. Moraga, M. Flores, R. Segura, S. Donoso, F. Marín, S. Bravo, and P. Häberle, Appl. Surf. Sci. **407**, 322 (2017).
[27] D. Josell, S. H. Brongersma, and Z. Tőkei, Annu. Rev. Mater. Res. **39**, 231 (2009).
[28] M. T. Bohr, Int. Electron Devices Meeting **1995**, 241 (1995).
[29] S. M. Rossnagel and T. S. Kuan, J. Vac. Sci. Technol. B **22**, 240 (2004).
[30] J. M. Purswani and D. Gall, Thin Solid Films **516**, 465 (2007).
[31] J. S. Chawla and D. Gall, Appl. Phys. Lett. **94**, 252101 (2009).
[32] J. S. Chawla, X. Y. Zhang, and D. Gall, J. Appl. Phys. **110**, 043714 (2011).
[33] J. S. Chawla, F. Gstrein, K. P. O'Brien, J. S. Clarke, and D. Gall, Phys. Rev. B **84**, 235423 (2011).
[34] J. S. Chawla and D. Gall, J. Appl. Phys. **111**, 043708 (2012).
[35] J. S. Chawla, X. Y. Zhang, and D. Gall, J. Appl. Phys. **113**, 063704 (2013).
[36] V. Timoshevskii, Y. Ke, H. Guo, and D. Gall, J. Appl. Phys. **103**, 113705 (2008).
[37] Y.-N. Zhao, S.-X. Qu, and K. Xia, J. Appl. Phys. **110**, 064312 (2011).
[38] T. Markussen, M. Palsgaard, D. Stradi, T. Gunst, M. Brandbyge, and K. Stokbro, Phys. Rev. B **95**, 245210 (2017).
[39] N. A. Lanzillo, J. Appl. Phys. **121**, 175104 (2017).

[40] G. Hegde, R. C. Bowen, and M. S. Rodder, Appl. Phys. Lett. **109**, 193106 (2016).
[41] A. Sanchez-Soares, S. L. T. Jones, J. J. Plombon, A. P. Kaushik, R. E. Nagle, J. S. Clarke, and J. C. Greer, Phys. Rev. B **94**, 155404 (2016).
[42] S. L. T. Jones, A. Sanchez-Soares, J. J. Plombon, A. P. Kaushik, R. E. Nagle, J. S. Clarke, and J. C. Greer, Phys. Rev. B **92**, 115413 (2015).
[43] Y. Ke, F. Zahid, V. Timoshevskii, K. Xia, D. Gall, and H. Guo, Phys. Rev. B **79**, 155406 (2009).
[44] V. Heine and D. Weaire, Solid State Phys.: Adv. Res. Appl. **24**, 249 (1970).
[45] D. Van Dyck, Ultramicroscopy **109**, 677 (2009).
[46] J. M. Soler, E. Artacho, J. D. Gale, A. García, J. Junquera, P. Ordejón, and D. Sánchez-Portal, J. Phys.: Condens. Matter **14**, 2745 (2002).
[47] J. Junquera, Ó. Paz, D. Sánchez-Portal, and E. Artacho, Phys. Rev. B **64**, 235111 (2001).
[48] E. Artacho, D. Sanchez-Portal, P. Ordejon, A. Garcia, and J. M. Soler, Phys. Status Solidi B **215**, 809 (1999).
[49] J. P. Perdew, K. Burke, and M. Ernzerhof, Phys. Rev. Lett. **77**, 3865 (1996).
[50] M. Fuchs and M. Scheffler, Comput. Phys. Commun. **119**, 67 (1999).
[51] M. Brandbyge, J.-L. Mozos, P. Ordejón, J. Taylor, and K. Stokbro, Phys. Rev. B **65**, 165401 (2002).
[52] Y. Liu, Z. Yuan, R. J. H. Wesselink, A. A. Starikov, M. van Schilfgaarde, and P. J. Kelly, Phys. Rev. B **91**, 220405 (2015).
[53] T. Gunst, T. Markussen, M. L. N. Palsgaard, K. Stokbro, and M. Brandbyge, Phys. Rev. B **96**, 161404(R) (2017).
[54] Y. Liu, A. A. Starikov, Z. Yuan, and P. J. Kelly, Phys. Rev. B **84**, 014412 (2011).
[55] K. M. Schep, P. J. Kelly, and G. E. W. Bauer, Phys. Rev. B **57**, 8907 (1998).
[56] R. A. Matula, J. Phys. Chem. Ref. Data **8**, 1147 (1979).
[57] T. Hehenkamp, W. Berger, J.-E. Kluin, C. Lüdecke, and J. Wolff, Phys. Rev. B **45**, 1998 (1992).
[58] J.-W. Lim, K. Mimura, and M. Isshiki, Appl. Surf. Sci. **217**, 95 (2003).
[59] P. A. Badoz, A. Briggs, E. Rosencher, F. A. d'Avitaya, and C. d'Anterroches, Appl. Phys. Lett. **51**, 169 (1987).
[60] D. Gall, J. Appl. Phys. **119**, 085101 (2016).
[61] T. Ando, A. B. Fowler, and F. Stern, Rev. Mod. Phys. **54**, 437 (1982).
[62] Y. Ke, K. Xia, and H. Guo, Phys. Rev. Lett. **100**, 166805 (2008).